Electronic Structure Effects in the Coupling of a Single Molecule with a Plasmonic Antenna

Fernando Aguilar-Galindo, Sergio Díaz-Tendero, Andrei Borisov

Electronic structure effects in the coupling of a single molecule with a plasmonic antenna

Fernando Aguilar-Galindo,[†] Sergio Díaz-Tendero,[†,‡,¶] and Andrei G. Borisov[*,§]

[†]*Facultad de Ciencias, Departamento de Química, Universidad Autónoma de Madrid, Ciudad Universitaria de Cantoblanco, 28049 Madrid, Spain*

[‡]*Instituto de Física de la Materia Condensada, Universidad Autónoma de Madrid, Ciudad Universitaria de Cantoblanco, 28049 Madrid, Spain*

[¶]*Institute for Advanced Research in Chemical Sciences (IAdChem), Universidad Autónoma de Madrid, Ciudad Universitaria de Cantoblanco, 28049 Madrid, Spain*

[§]*Institut des Sciences Moléculaires d'Orsay, UMR 8214 CNRS-Université Paris-Sud, Bâtiment 520, 91405 Orsay Cedex, France*

E-mail: andrei.borissov@u-psud.fr

Phone: +33 (0)1 69157697

Abstract

Miniaturisation of plasmonics devices and possibility to address single molecule quantum emitters in plasmonic cavities allows one to approach a regime where the characteristic sizes of the system are at the scale of molecular dimensions. In such a situation, the actual spatial profile of the transition electron density affects the coupling between molecular excitons and metal (nano)objects. Using a quantum approach we address the energies and lifetimes of excited states of the zinc phthalocyanine dye molecule placed in the nm vicinity of a plasmonic antenna. We demonstrate that the interaction between molecular excitons and a metal nanoparticle reflects the gross features of the

atomic structure in the molecule. The possibility to "look" inside the molecule does not require the presence of atomic scale probes at the surfaces of plasmonic nanoparticles, that would lead to the corresponding localization of the optical field. We show that the quantum emitter itself simultaneously generates highly localized fields and probes them via self-interaction.

Introduction

The coupling of excited electronic states of quantum emitters (QE), such as semiconductor quantum dots or organic molecules, with collective plasmon modes of metallic nanostructures is of interest for various applications such as information transfer technology, active optical devices, superluminescence, and sensing. Controlling the plasmon-exciton coupling strength via an effective volume of the plasmon mode, a quality factor, and an energy of the plasmon resonance allows one to engineer the exciton dynamics and the optical response of the system.[1–8] In particular, in the strong coupling regime the mixed plasmon-exciton states are formed with characteristic Rabi splitting of their frequencies corresponding to the transfer of the excitation energy back and forth between the plasmon mode and the QE.[9–19] Hybrid structures formed by a QE and a plasmonic system undergo dramatic changes in the optical response as compared to the individual components separately.[7,8,20]

Recent experimental advances allowed to place molecules in ultranarrow plasmonic gaps formed by metal nanoparticles or by junctions between a surface and the tip of a scanning tunneling microscope (STM). In these situations, shrinking an effective plasmon mode volume leads to a huge increase of the interaction strength between molecular emitters and plasmonic system.[9–16] An STM junction provides an another advantage: possibility of spatial control of both excitation and photon emission processes owing to electron tunneling and plasmon-exciton coupling. Atomic scale resolved Raman spectroscopy[21–25] and lumi-

nescence[26–34] have been thus reported. This offers unprecedented opportunities for single molecule analysis and quantum sources of light.

By analogy with atomic resolution in the standard tunneling mode,[35,36] spatial control of the plasmon exciton coupling in STM junctions and plasmonic cavities can be associated with sub-nm protrusions at metal surfaces within the gap.[37–39] The presence of such atomic-scale structures allows to localize optical fields and to bridge the difference between the molecular scale (Å) and typical sizes of the hot spots $s = \sqrt{Rd_g}$,[40] where $R \sim 20$ nm is the curvature radius of the tip and $d_g \sim 2$ nm is the width of the gap. Recent calculations indeed demonstrate the corresponding localisation of the optical fields,[38,41] allowing angstrom scale resolved control of the exciton properties.[39] At the same time, the molecular QE itself represents an atomic scale structure with corresponding localization of the fields associated with an exciton. When the distance between the QE and the surface(s) of plasmonic nanoparticle(s) approaches molecular dimensions, one might expect that exciton couplings with the plasmonic system become sensitive to the molecular structure in general, and to the actual spatial profile of the electronic density associated with an exciton in particular. Can this intrinsically QE related effect lead to the spatially resolved exciton coupling with the plasmonic system?

In this work, we answer the above question taking as example the zinc phthalocyanine dye molecule (ZnPc) placed in the vicinity of a plasmonic nanoantenna. Using the random phase approximation[42] within the time dependent density functional theory[43,44] we address the molecular electronic structure effects on the exciton coupling with a metal nanoparticle. For the molecule-nanoantenna distances in the nm range we show that the excitation energy, the decay rate, and the induced molecular dipole reflect the gross features of the atomic arrangement with respect to the nanoantenna. For the studied molecule, with D_{4h} symmetry, this result is in sheer contrast with the point dipole approximation for QE. This effect found in our work emerges owing to the finite spatial profile of the transition electron density associated with an exciton. As such, it does not require localization of the incident fields

and it can be observed even with flat metal surfaces. In light of these results we discuss the possibility of spatial imaging of molecular excitation with nm size tips.

Methods

To reveal and to understand the electronic structure effects in exciton/nanoparticle coupling it is convenient to use as a reference results obtained with a point dipole description of the quantum emitter.[1,2,45–50] Within the point dipole approximation, the spatial profile of the excited molecular orbitals is neglected. Only the leading term given by the transition dipole moment is retained to describe the interaction with metal nanoparticle. While quantum chemistry methods for the interaction between excited molecules and surfaces have been developed in the context of plasmonics,[51–58] an intuitively transparent and computationally efficient point dipole approximation is still widely used. It allows to describe the experimental data for situations where the emitter/nanoparticle separations are such that the quantum effects can be neglected.

In Fig. 1 we show a sketch of the geometry of the studied system including the atomic structure of the ZnPc molecule. The optical excitations in the ZnPc molecule correspond to the transitions between the ground state and two degenerate excited states with transition dipoles $\mathbf{p}_x$ and $\mathbf{p}_y$ oriented along the x and y molecular axes within the molecular (x, y)-plane. Because of the D_{4h} symmetry $p_x = p_y = \mu$, and the molecular in-plane polarisability is given by a scalar value $\alpha(\omega)$. The polarizability perpendicular to the molecular plane is small and can be neglected. Thus, the response of the individual ZnPc molecule to the field of an incident electromagnetic plane wave, $\mathbf{E}^{in}$, polarized within the molecular plane, is independent of the molecular orientation. The induced dipole is oriented along the incident field, and it is given by $\mathbf{d} = \alpha(\omega)\mathbf{E}^{in}$, where $\alpha(\omega) = \frac{\mu^2}{\omega_0 - \omega - i\eta/2}$ is the molecular polarisability (atomic units are used unless otherwise stated). The transition dipole moment $\mu = 5.84$ a$_0$ (a$_0 = 0.53$ Å is the Bohr radius), and the transition frequency $\omega_0 = E_e - E_g = 1.796$ eV

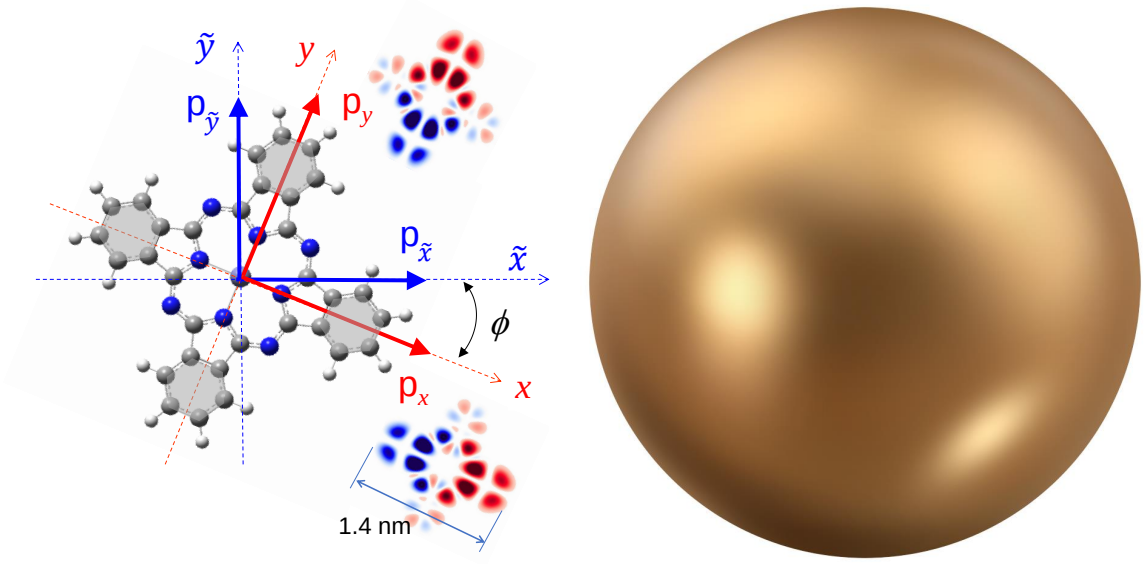

Figure 1: Sketch of the considered geometry (top view). The ZnPc molecule is placed in the equatorial plane of the spherical metal nanoparticle. The molecular orientation with respect to the nanosphere is given by the molecular axis rotation angle ϕ. The x- and y- axes define a molecular reference frame. The $\tilde{x}$- and $\tilde{y}$- axes define a natural frame with $\tilde{x}$-axis along the direction connecting molecular and nanoparticle centers. The external carbon rings of the molecule are hatched with grey color. The dipole moments of the molecule, p_x and p_y, induced by the optical excitation are associated with transition charge densities shown with red (positive) and blue (negative) bi-color images. The linear combinations of p_x and p_y excitons are denoted as $p_{\tilde{x}}$ and $p_{\tilde{y}}$. These states are oriented along the $\tilde{x}$- and $\tilde{y}$ axes of the natural frame. In the point dipole picture, the $p_{\tilde{x}}$ and $p_{\tilde{y}}$ excitons are the eigenstates of the system not coupled by the interaction with nanoparticle.

are obtained here from quantum chemistry calculations using the Gaussian09 package[59] with the HSE06 hybrid exchange-correlation functional.[60–62] The parameter η stands for a (small) attenuation because of the radiation losses and intrinsic broadening effects. In what follows, for the molecule placed in nm vicinity from the metal surface, the nonradiative decay because of the losses in metal dominates the broadening of the excited state and (small) η can be neglected.

When placed in front of the plasmonic nanoparticle(s), the molecule experiences the field induced in response to its own dipole. The total field acting on the molecule is then given by $\mathbf{E}^{tot} = \mathbf{E}^{ext} + \mathbf{G}\mathbf{d}$. Here, $\mathbf{E}^{ext}$ is the sum of the incident field and the field created by the metal nanoparticle in response to an incident field, and $\mathbf{G}\mathbf{d}$ is the field induced in response

to the molecular dipole, where $\mathbf{G}$ is the Green's tensor. From the symmetry of the problem it is convenient to use the natural $(\tilde{x}, \tilde{y})$ frame (see Fig. 1). Within this frame the components of the induced dipole can be found from (see Supporting Information)

$$d_j = \frac{\alpha(\omega) E_j^{ext}}{1 - \frac{4\pi}{c^2}\omega^2 \alpha(\omega) G_j(\mathbf{R}, \mathbf{R})}, \quad j = \tilde{x}, \tilde{y}, \tag{1}$$

where j stands for the projection of the vector on the corresponding axis, and $G_j(\mathbf{R}, \mathbf{R})$ is the corresponding component of the diagonal Green's tensor taken at the molecular position $\mathbf{R}$. From the point dipole approximation it follows that the excitons with transition dipole moments $p_{\tilde{x}}$ and $p_{\tilde{y}}$ oriented along the axes of the natural frame are the eigenstates of the system. These excitons are not coupled by the surface, and their complex eigen-energies are given by

$$\Omega_j = \omega_0 - \frac{4\pi}{c^2}\omega^2 \alpha(\omega) G_j(\mathbf{R}, \mathbf{R}), \quad j = \tilde{x}, \tilde{y}. \tag{2}$$

The exciton energy is given by the real part of Ω, and the exciton half-width is given by the imaginary part of Ω. As an important result *within the point dipole approximation the ZnPc exciton coupling with plasmonic nanoparticle does not depend on the molecular axis rotation angle* ϕ. This is in contrast with linear molecules, where the alignment of the transition dipole results in molecular orientation dependence of the exciton coupling with the nanostructure, already at the point dipole approximation level. The ZnPc is then well suited to address quantum effects related with realistic spatial profile of the transition electron density.

To include the effect of molecular electronic structure on the energies and lifetimes of excited states of the molecule in a plasmonic environment we apply a quantum approach based on the Kohn-Sham (KS) formulation of the time-dependent density functional theory (TDDFT).[43,44] This allows to go beyond the point dipole approximation and to account for the actual spatial profile of the transition electron density. The time-dependent KS orbitals are sought in the basis of the ground ψ_g and degenerate excited $\psi_{x,y}$ molecular orbitals. The x, y indices refer here to the orientation of the transition dipole (see Fig. 1). As explained

in the Supporting Information, the exciton eigenstates of the system are obtained from the non-hermitian eigenvalue problem as combination of the p_x and p_y molecular excitons.

$$\begin{vmatrix} \omega_0 - \omega + \langle \psi_x | e\varphi(\omega, \psi_g\psi_x) | \psi_g \rangle & \langle \psi_x | e\varphi(\omega, \psi_g\psi_y) | \psi_g \rangle \\ \langle \psi_y | e\varphi(\omega, \psi_g\psi_x) | \psi_g \rangle & \omega_0 - \omega + \langle \psi_y | e\varphi(\omega, \psi_g\psi_y) | \psi_g \rangle \end{vmatrix} = 0 \tag{3}$$

Complex-valued solutions of Eq. (3) provide frequencies and decay rates of the excitations. The potential $\varphi(\omega, \psi_g\psi_m)$, where $m = x, y$, is given by the response of the metallic nanostructure at the presence of the transition charge density $\delta n_m(\omega) = 2e\psi_g\psi_m$ placed in front of its surface. Here, $e = -1$ is an electron charge, and factor 2 accounts for the spin degeneracy. The non-retarded approximation consistent with the small characteristic size of the system is used. The potential $\varphi(\omega, \psi_g\psi_m)$ is calculated from the solution of Poisson's equation $\nabla\varepsilon(\mathbf{r}, \omega)\nabla\varphi(\omega, \psi_g\psi_m) = -4\pi\delta n_m(\omega)$. $\varepsilon(\mathbf{r}, \omega)$ is the coordinate and frequency dependent dielectric function. For the metal permittivity we used the tabulated empirical data[63,64] as well as the Drude model. Further details are given in Supporting Information.

At this point it is worth stressing that the quantum model applied in this study is aimed at capturing the main physics linked with finite spatial distribution of the excited electron density. More advanced treatments[51–58] would be needed to account for the perturbation of the ground and excited electronic orbitals in vicinity of a metal.

Results and discussion

Before the quest for molecular structure effects in QE coupling with plasmonic nanoparticles it is instructive to consider the ZnPc molecule in front of a flat metal surface. This is a reference system in the sense that there is no field confinement by the localized plasmon modes or by the surface nanostructures. Thus, if found, the dependence of the exciton properties on molecular orientation can be considered as a clear cut demonstration of the effect of the spatial extension of the excited electron density. In Fig. 2 we compare energies

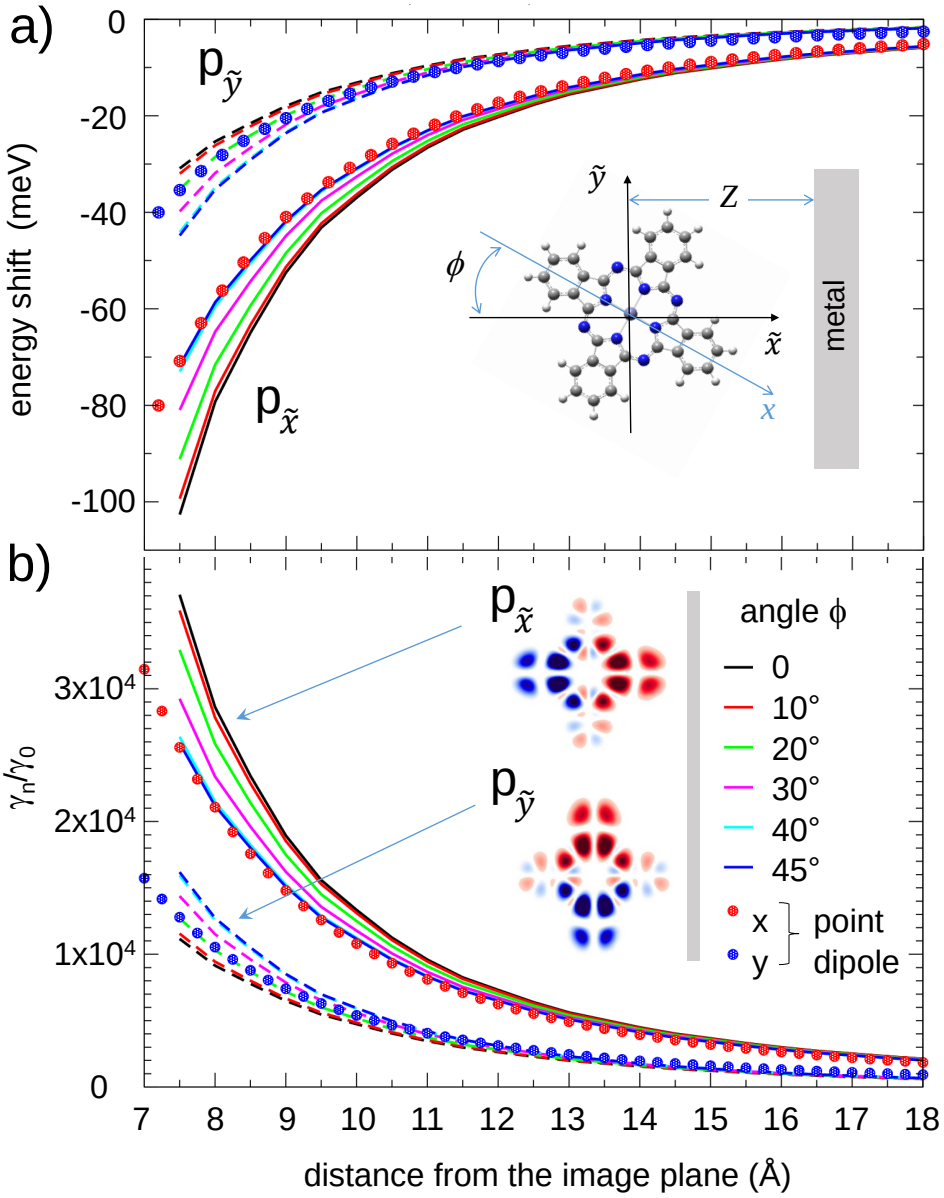

Figure 2: ZnPc molecule in front of the flat Al surface. Energy and lifetime of ZnPc molecular exciton states obtained from the quantum (lines) and point dipole (dots) calculations. Results are shown as function of molecule-surface distance Z for different molecular axis rotation angles ϕ. Solid (dashed) lines are used for the molecular exciton states of $p_{\tilde{x}}$ ($p_{\tilde{y}}$) character. a) Energy shift of molecular exciton with respect to the excitation energy of the free-standing ZnPc molecule ($\omega_0 = 1.796$ eV). b) The decay rate enhancement by the metal γ_n/γ_0, where the radiative decay rate of the individual ZnPc molecule in vacuum $\gamma_0 = \frac{4\omega_0^3}{3C^3}\mu^2 = 7 \times 10^{-8}$ eV. The inserts show the geometry of the system [panel a)], and the transition charge density of molecular excitons for $\phi = 0$ [panel b)].

[panel a)] and decay rates [panel b)] of the ZnPc excitons calculated using the point dipole approximation, and the random phase approximation within the time dependent density functional theory (hereafter referred as quantum model). The results obtained for different molecular axis rotation angles ϕ are shown as a function of the distance Z between the molecule and the flat Al metal surface. The geometry of the system is such that the ZnPc molecular plane is perpendicular to the metal surface [see Fig. 1) and an insert of Fig. 2a)].

Within the point dipole model, the p_x and p_y molecular excitons form the symmetry adapted $p_{\tilde{x}}$ and $p_{\tilde{y}}$ linear combinations oriented along the $\tilde{x}$ and $\tilde{y}$ axes of the "natural" frame. Irrespective of the molecular axis rotation angle ϕ, these are the eigenstates of the problem not coupled by the surface response potential. With decreasing the molecule-surface distance Z the exciton energy redshifts, and the exciton decay increases following a $1/Z^3$ dependence determined by the interaction between the dipole and its image created by the metal surface (see Supporting Information for further details). The calculated orders of magnitude enhancement of the decay rate as compared to the free standing molecule stems from the nonradiative decay channel associated with losses to electron hole pair excitations in the metal.[1–3] As expected, the interaction with the metal is stronger for the $p_{\tilde{x}}$ exciton, with its transition dipole oriented perpendicular to the surface.

While the point dipole model provides a good order-of-magnitude estimate to the quantum results, it completely misses the strong molecular orientation dependence of the exciton-metal surface coupling as found in the quantum model calculations. When the distance to the metal surface Z becomes comparable to the spatial extension of the excited molecular orbital ($\sim$ 1.4 nm), the results of the quantum approach show a clear variation with ϕ. This is because the higher order multipole moments of the transition charge density contribute to the metal response in the presence of an excited molecule. The $p_{\tilde{x}}$ and $p_{\tilde{y}}$ excitons are hybridized. Depending on molecular axis angle ϕ, the $\cos(\beta)p_{\tilde{x}} + \sin(\beta)p_{\tilde{y}}$ and $-\sin(\beta)p_{\tilde{x}} + \cos(\beta)p_{\tilde{y}}$ hybrids are formed with β being the effective rotation angle. Only in the high symmetry cases, for $\phi = n\pi/4$ (n-integer), the pure $p_{\tilde{x}}$ ($p_{\tilde{y}}$) states are retrieved.

In the considered range of molecule-surface distances, the high order moments of the transition density are at the origin of the dependence of the results on the molecular axis rotation angle. At the same time, the dipole moment of the transition density provides a leading contribution to the metal response. The β-parameter is small; we obtained that $\beta << \phi$. The transition dipole is not directed along the molecular axis, and the main $p_{\tilde{x}}$ ($p_{\tilde{y}}$) character of the excitonic states predicated by the point dipole model is preserved. This is also consistent with grouping results in Fig. 2 in two distinct series when the molecular axis is rotated.

It is worth noting that the results in Fig. 2 are shown down to molecule surface distance of 7 Å, to cover large range of the variation of exciton energies and widths, and consistent with the typical range of distances when discussing plasmon field confinement effects on sub-nm resolution.[37–39] However, in practice, for the present geometry with one of the excited orbitals pointing towards the surface, for molecular surface distances below 10-12 Å resonant electron tunneling between this orbital and the metal[65] can become important. The resonant tunneling leads to quenching of the excited state population and it concerns primary the width of the excited state, while the energy is affected to a smaller extent as has been shown in the theoretical studies of electron transfer between atomic species and metal surfaces.[66]

Further insight into the effect of the excited electron density distribution on the exciton/metal coupling can be gained from the results presented in Fig. 3. We show the energies [panel a)] and decay rates [panel b)] of molecular excitons as a function of the molecular axis rotation angle ϕ for a fixed molecule-surface distance of $Z = 1$ nm. Energies and decay rates of the molecular excitons vary periodically with ϕ reflecting the ZnPc symmetry. For the $p_{\tilde{x}}$ exciton the amplitude of the energy variation equals to ~ 7 meV and the variation of the decay rate reaches ~ 10 %. This is comparable to the earlier results reported for the ZnPc molecule in the narrow plasmonic gap decorated with an atomic scale protrusion.[39] The $p_{\tilde{y}}$ exciton not reported in[39] is less coupled to the surface and features smaller variations in energy and width with ϕ.

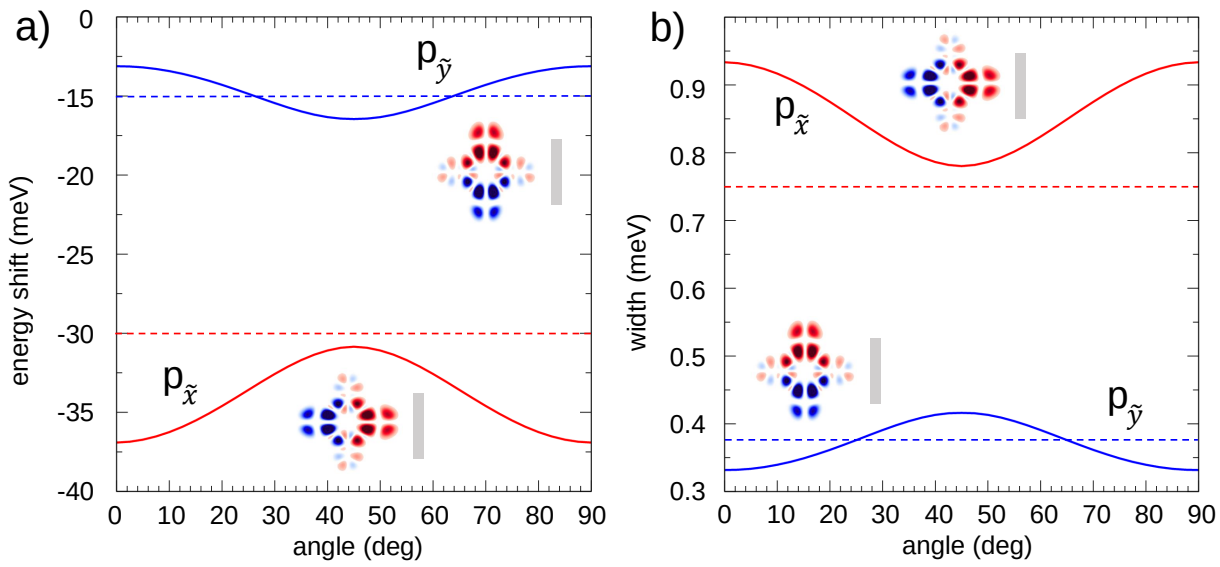

Figure 3: Properties of ZnPc molecular excitons calculated with quantum approach as a function of the rotation angle ϕ for a fixed molecule-surface distance $Z = 1$ nm. Results for the exciton states with $p_{\tilde{x}}$ ($p_{\tilde{y}}$) character are shown with red (blue color). The corresponding transition charge densities are shown in panels a) and b) for the ϕ=0 case. Panel a): energy shift with respect to the transition in the free-standing molecule. Panel b): width of the exciton resonances (nonradiative decay rates). Dashed horizontal lines in panels a) and b) of the figure show the results of the calculation using point dipole model.

Interestingly, the $p_{\tilde{x}}$ and $p_{\tilde{y}}$ results show ϕ oscillations in opposite phase. Thus, for the $p_{\tilde{x}}$-case interaction with the metal maximizes for the molecule axis pointing at the surface at $\phi = 0$ and $\phi = 90°$, while for the $p_{\tilde{y}}$ exciton the attractive interaction maximizes at $\phi = 45°$. This result can be understood from the atomistic structure of the molecule sketched in Fig. 1. For $\phi = 0$ the $p_{\tilde{x}}$ exciton is oriented along the molecular axis. The external carbon ring is brought in proximity of the surface maximising the interaction. Similarly, the $\tilde{p}_y$ exciton at $\phi = 45°$ is given by the linear combination $(\mathbf{p}_x + \mathbf{p}_y)/\sqrt{2}$ and part of the transition density is distributed over the two external carbon rings oriented towards the surface so that the interaction reaches its maximum.

The molecular axis rotation angle dependence of the exciton energy and width allows to illustrate the qualitative difference between the quantum description, taking into account the realistic electron density distribution of the excited state, and the point dipole approximation. At the same time, the quantum effect discussed in this paper obviously leads to

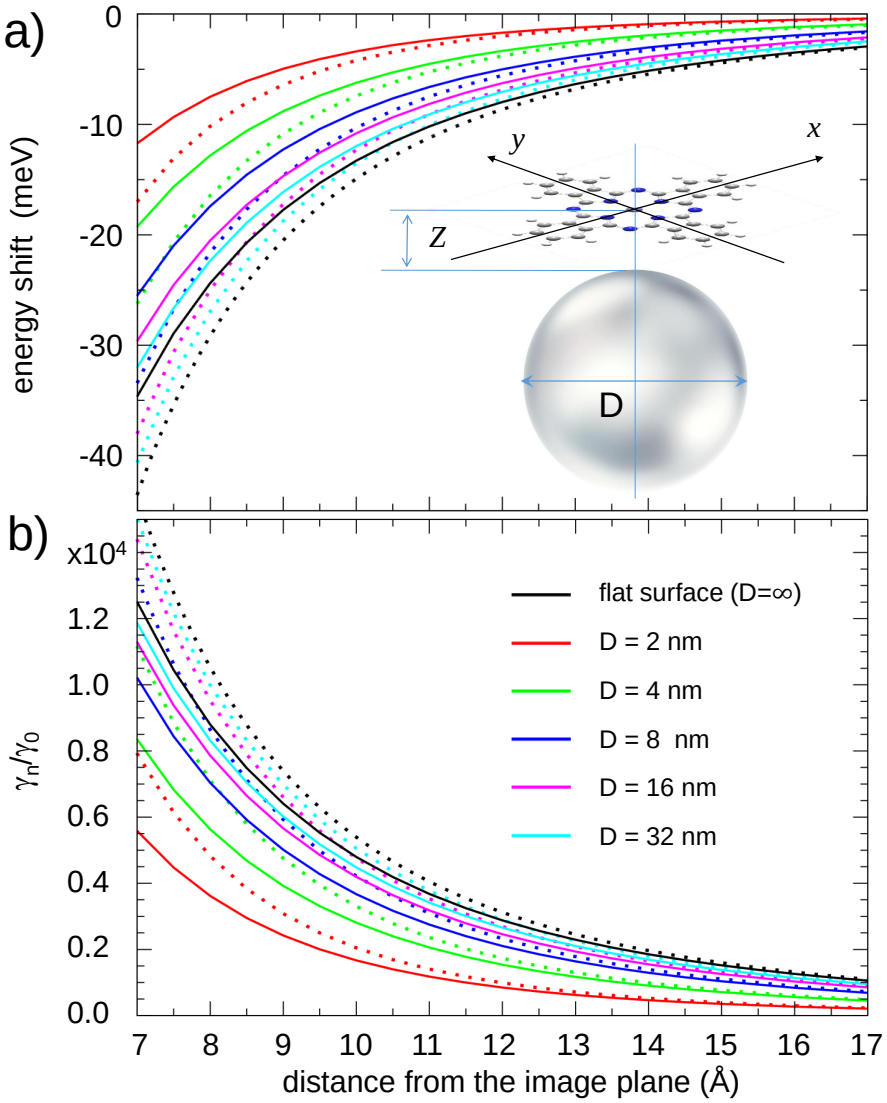

Figure 4: ZnPc molecule with molecular plane parallel to the flat Al surface or grazing to the surface of spherical Al nanoparticle. Energy and lifetime of ZnPc molecular exciton states obtained from the quantum (solid lines) and point dipole (dotted lines) calculations. Results for degenerate p_x and p_y molecular exciton states are shown as a function of molecule-surface distance Z for the Al nanoparticles of different diameter. The insert in [panel a)] shows the geometry of the system, and the insert in [panel b)] explains the color code. a) Energy shift of molecular exciton with respect to the excitation energy of the free-standing ZnPc molecule ($\omega_0 = 1.796$ eV). b) The decay rate enhancement by the metal γ_n/γ_0, where the radiative decay rate of the individual ZnPc molecule in vacuum $\gamma_0 = \frac{4\omega_0^3}{3C^3}\mu^2 = 7 \times 10^{-8}$ eV.

the quantitative differences with the point dipole model even for those geometries where the excitonic states are degenerated and no orientational effects can be observed. For example,

this is the case for the molecule oriented such that molecular plane is parallel to the flat Al metal surface, or it is grazing to the surface of Al spherical nanoparticle as shown in Fig. 4. Since the extension of molecular orbitals is very small in the direction perpendicular to the molecular plane, no electron tunneling is expected down to the shortest distances shown in the figure.

Because of the symmetry the excited molecular states are degenerated and, obviously, no effects of the molecular axis rotation angle can be observed. In fact, for the flat metal surface the quantum results for the width and broadening of the excited state are very close to those obtained in Fig. 1 for the $p_{\tilde{y}}$ exciton also oriented parallel to the surface albeit with different orientation of the molecular plane (the point dipole results are obviously identical for these two cases). For the finite size Al nanoparticle, the molecule/nanoparticle interaction increases with the nanoparticle diameter D, approaching the flat surface ($D = \infty$) limit. At large distances the results scale as D^3, reflecting the scaling of the polarisability of an Al sphere. Similar to the results reported in Fig. 1, the differences between the quantum and point dipole calculations tend to zero at large molecule surface distances Z, larger than the molecular dimensions. Thus, the energy shift of molecular exciton with respect to the excitation energy of the free-standing ZnPc molecule can be approximated with a $1/Z^3$ dependence, reflecting the interaction between molecular dipole and its image charge in the metal. At the same time, the difference between the quantum and classical results, caused by the higher moments in the transition density, decreases as $1/Z^4$ with increasing Z.

In this paper, we are however primarily interested in the orientational effects opening the possibility of spatially resolved imaging with underlying mechanisms under debate presently. In this respect, the insights provided by the reference calculations of the ZnPc molecule in front of the flat metal surface alow to understand a more complex situation when the ZnPc molecule interacts with plasmonic nanoobjects. In Fig. 5 we show the absorption spectra calculated with the quantum approach for the ZnPc molecule at $Z = 1$ nm distance from a spherical gold nanoparticle of 5 nm radius. In this weak coupling regime the main absorption

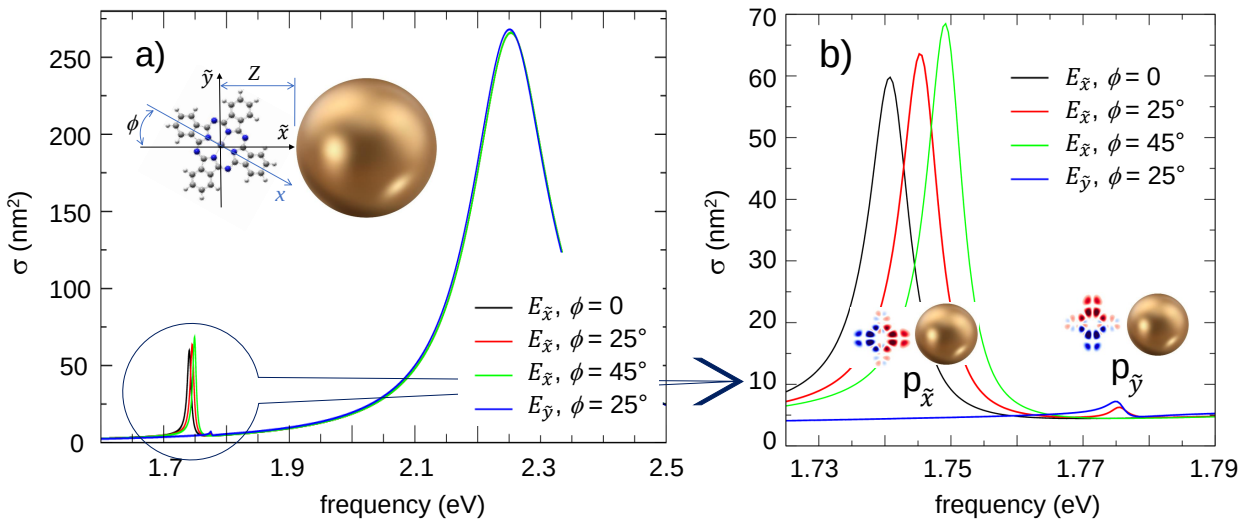

Figure 5: ZnPc molecule in front of the gold sphere of 5 nm radius, the molecule-surface distance $Z = 1$ nm. The molecular plane coincides with equatorial plane of the nanoparticle as schematically shown in the insert of panel a) (top view). The $\tilde{x}$-axis contains geometrical centers of the molecule and nanoparticle. Panels a) and b) of the figure show an absorption spectra obtained from the quantum approach for different rotation angles ϕ and different polarisations of the incident electromagnetic plane wave with electric field vector oriented along the $\tilde{x}$ ($E_{\tilde{x}}$) or the $\tilde{y}$ ($E_{\tilde{y}}$) axis. Color codes are explained in the inserts. Panel a) gives the results within the wide frequency range while panel b) zooms into the molecular exciton. The inserts of panel b) show the transition charge densities of molecular excitons for $\phi = 0$.

resonance seen in the panel a) for $\omega = 2.25$ eV corresponds to the excitation of the dipolar plasmon mode of the nanoparticle. It is little sensitive to the polarization of the incident field and to the molecular axis rotation angle. The absorption features close to 1.7 eV result from molecular excitons. Panel b) provides a zoom into this lower frequency range. For the $\tilde{x}$-polarized incident field, the exciton with $p_{\tilde{x}}$-character is associated with the strongest absorption. The evolution of its energy and width (not shown) with the ϕ-angle is similar to that found in front of the flat metal surface. The weak absorption feature at $\omega = 1.775$ eV, obtained with $\tilde{x}$-polarized incidence for $\phi = 25°$, is ascribed to the exciton with $p_{\tilde{y}}$ character. Because of the hybridization between the $p_{\tilde{x}}$ and $p_{\tilde{y}}$ excitons the transition dipole is slightly rotated away from the $\tilde{y}$-axis. Thus, it couples with $\tilde{x}$-polarized field for $\phi = 25°$, but not for the high symmetry cases ($\phi = 0,\ 45°$). Albeit slightly shifted in frequency because of the Fano profile,[67,68] the same resonance is obtained for $\phi = 25°$ with $\tilde{y}$-polarized incoming field.

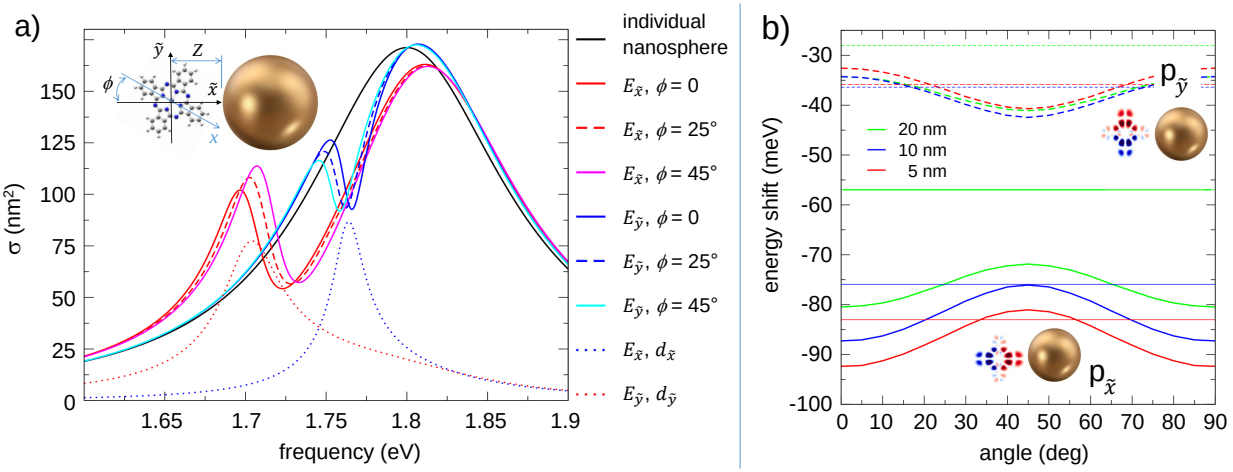

Figure 6: ZnPc molecule in front of the model metal sphere of the 5 nm radius as sketched in the insert of panel a). The dipolar plasmon of the individual nanosphere is at $\omega_D = 1.8$ eV. Panel a): Absorption spectra obtained from the quantum treatment for the incident electromagnetic plane wave polarized along $\tilde{x}$ ($E_{\tilde{x}}$) or $\tilde{y}$ ($E_{\tilde{y}}$) axis. Results are shown for different molecular axis rotation angles ϕ. For the reference we also show the absorption spectra of an individual nanosphere as well as the $d_{\tilde{x}}$ ($d_{\tilde{y}}$) components of the molecular dipole induced for the $\phi = 0$ case by the $\tilde{x}$ ($\tilde{y}$) polarised external field. Panel b): Energy shift of the excitons with $p_{\tilde{x}}$ (solid lines), and $p_{\tilde{y}}$ (dashed lines) character with respect to the transition in free standing ZnPc molecule. Results are shown as function of the rotation angle ϕ for different nanoparticle radii (5, 10, and 20 nm) as explained in the insert. Thin horizontal lines indicate results of the point dipole approximation. The inserts show the transition charge densities of molecular excitons for $\phi = 0$.

The situation when the molecular exciton and dipolar plasmon of the spherical nanoparticle are at resonance allows to study the effect of the molecular orientation in the strong coupling regime. In Fig. 6 we show the absorption spectra for the ZnPc molecule located at 1 nm from the surface of the model metal nanosphere. The metal dielectric function has been described with the Drude model, where the bulk plasmon frequency has been set such that the dipolar plasmon of the nanoparticle is at $\omega_D = 1.8$ eV. I.e. it is at resonance with excitons of the free standing ZnPc molecule. The molecule is located in the equatorial plane of the nanosphere as sketched in the insert of Fig. 6a).

Depending on the polarisation of the incident plane wave, the $p_{\tilde{x}}$ and $p_{\tilde{y}}$ excitons lead to pronounced Fano structures[67,68] in the absorption spectra. The $p_{\tilde{x}}$ exciton with transition dipole pointing in the direction of nanoparticle, presents a stronger coupling with the

latter as compared to the $p_{\tilde{y}}$ exciton, oriented grazingly to the nanoparticle surface. This is reflected in a more pronounced variation of the adsorption cross section at the $p_{\tilde{x}}$ exciton energy, and in a larger exciton energy redshift from the free-molecule transition (1.796 eV). Analysis of the absorption spectra of individual metal nanoparticles and of the frequency dependence of the induced molecular dipoles shows that the $p_{\tilde{y}}$ exciton is associated with an absorption minimum. The $p_{\tilde{x}}$ exciton is associated with a more complex profile of the absorption spectra. The phase relation between the molecular and nanoparticle contributions to the total dipole is such that the induced molecular dipole resonance in this case does not correspond to the minimum or to the maximum of the total absorption cross section. Finite spatial extension of the transition charge densities leads to a clear dependence of the exciton/nanoparticle coupling on the molecular orientation. This can be nicely observed as a shift of the corresponding Fano profiles in absorption spectra with the molecular axis rotation angle ϕ.

Detailed information on the ϕ - dependence of the energies of the exciton modes is presented in Fig. 6b). In this figure we compare quantum and point dipole results obtained for the ZnPc molecule located at 1 nm from spherical nanoparticles with different radii: 5, 10, and 20 nm. The same Drude model dielectric function of the metal has been used as for the results shown in panel a). In overall, because of the orientation of transition dipole, the $p_{\tilde{x}}$ exciton experiences larger energy redshift than the $p_{\tilde{y}}$ exciton. Increasing the nanoparticle radius decreases the exciton/plasmon coupling. The exciton energy blueshifts towards the free-standing molecule value. Inline with findings for the flat metal surface, the quantum results show a periodic oscillation with an opposite phase for $p_{\tilde{x}}$ and $p_{\tilde{y}}$ states. The ~ 10 meV oscillation amplitude also decreases with increasing the nanoparticle radius, i.e. when the exciton coupling with the nanoparticle is reduced.

The similar trends obtained for the ZnPc molecular excitons interacting with flat metal surfaces and with spherical plasmonic nanoparticles result from the common underlying mechanism that can be understood as follows. The molecular excitation from the ground

to excited states is associated with transition electron density characterized by its multipole moments. In typical conditions, the interaction with a plasmonic (nano)structure is determined by the dipolar polarisation. However, when the distance to the metal becomes comparable with the spatial extension of the excited molecular orbitals the situation changes. The higher order multipole moments of the transition density contribute to the response of the metal in the presence of the QE. The molecular exciton plays simultaneously the role of the source and the probe of highly localized fields, so that the exciton/metal coupling is sensitive to the gross features of atomic arrangements in the molecule. Similar effect of the self-interaction was proposed in the context of SERS studies.[69] Thus, the spatial sensitivity reported here is not linked with the existence of atomic size protrusions often evoked as localized probes of an electronic structure[35,36] or optical properties.[37–39]

We further illustrate our findings with an example of the ZnPc molecule scanned with a spherical gold nanoparticle of diameter D. The geometry of the system is sketched in Fig. 7a). The nanoparticle scans the molecule in the (x, y) plane which is parallel to the molecular plane. The separation between the nanoparticle and molecular plane is kept constant 0.5 nm. At this flat geometry, taking into account out-of-plane extension of molecular orbitals calculated here the electron tunneling might be neglected. Another important argument in favour of the above choice of the separation distance is the possibility of the direct comparison with earlier published results.[39] Similar to the above considered cases in this paper, the p_x, and p_y molecular excitons are coupled by the interaction with the nanoparticle. Their linear combinations form the excitonic eigenmodes of the system. As stems from the symmetry of the problem, one of the eigenmodes is associated with the transition dipole oriented preferentially towards the center of the projection of the nanosphere in the molecular plane. By continuity with discussion in this paper we will assign this exciton as $p_{\tilde{x}}$. Another hybridized state, assigned as $p_{\tilde{y}}$, is associated with a transition dipole moment in an orthogonal direction. The transition charge densities of the modes are sketched in the inserts of Fig. 7b).

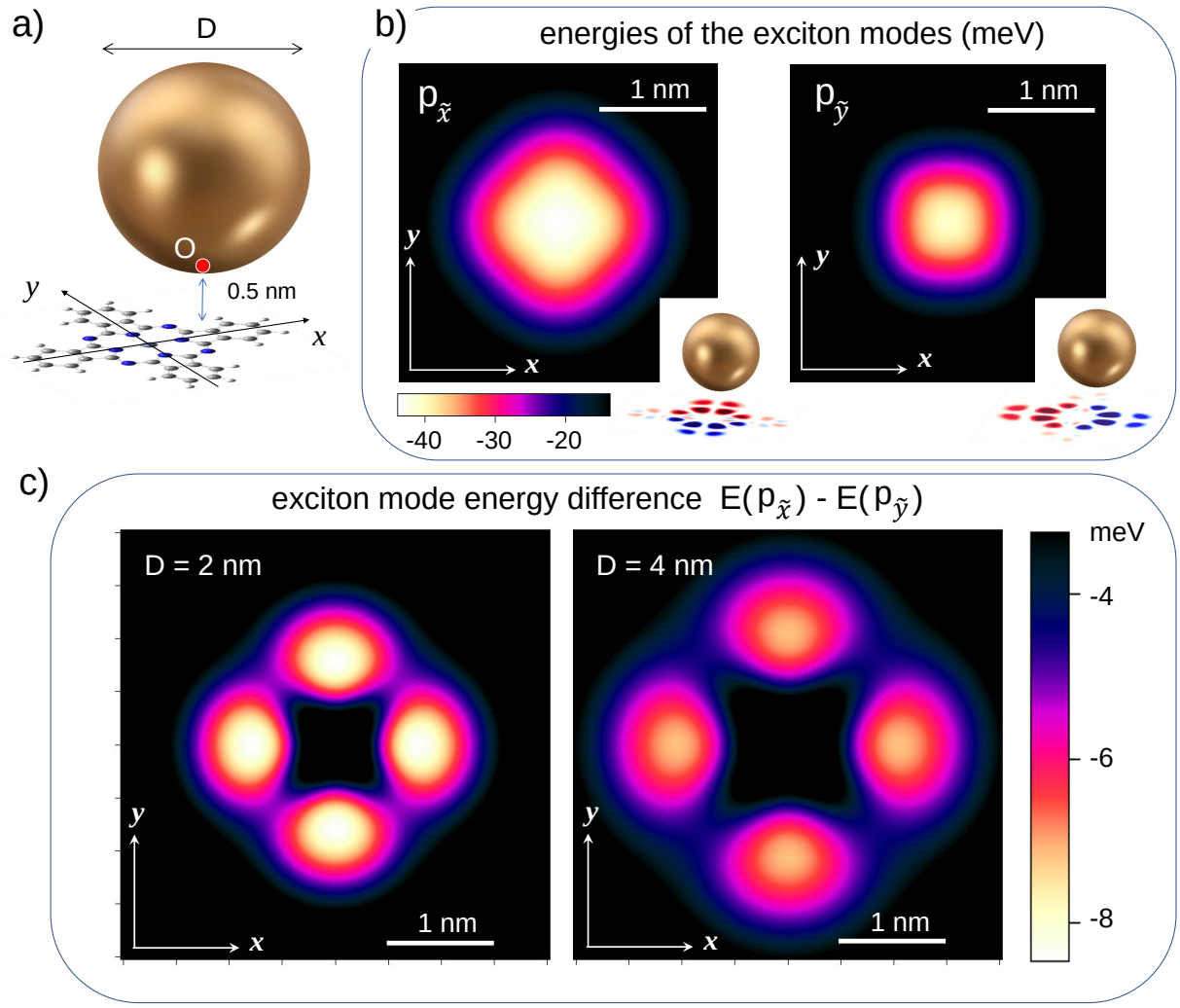

Figure 7: ZnPc molecule scanned by the spherical gold nanoparticle of diameter D. As sketched in panel a), the nanoparticle is moved in the plane parallel to the molecular plane. The separation between the molecular plane and the "analysis plane" is 0.5 nm. Panel b): contour maps of the energies of the exciton modes with $p_{\tilde{x}}$ and $p_{\tilde{y}}$ character. Results are shown as a function of the position of the $D = 2$ nm gold nanosphere. The inserts of the figure show the transition charge density distribution of the corresponding exciton modes. Panel c): contour maps of the energy difference between the exciton modes with $p_{\tilde{x}}$ and $p_{\tilde{y}}$ character, $E_{p_{\tilde{x}}} - E_{p_{\tilde{y}}}$. Results are shown as function of the position of the $D = 2$ nm gold nanosphere (left image) and $D = 4$ nm gold nanosphere (right image).

In Fig. 7b) we also show the spatial maps of the energies of the exciton eigenmodes. The ZnPc molecule is scanned with $D = 2$ nm gold nanoparticle. The rounded square images are obtained reflecting molecular orientations and its D_{4h} symmetry. The energy maps of the $p_{\tilde{x}}$ and $p_{\tilde{y}}$ excitons are rotated by 45° with respect to each other. This image

rotation reflects different dependence of the exciton/nanoparticle coupling on the molecular orientation as discussed earlier. For the $p_{\tilde{x}}$ exciton the interaction with the nanoparticle maximizes when the nanosphere scans a molecular axis. For the $p_{\tilde{y}}$ exciton the interaction is strongest at the diagonal between the x and y directions. The image obtained with $p_{\tilde{y}}$ exciton mode appears to have smaller lateral extensions because of the smaller interaction with nanoparticle. For the fixed radial position of the nanosphere $r = \sqrt{x^2 + y^2} = 0.75$ nm, we obtained ~ 2 meV amplitude of the variation of the $p_{\tilde{x}}$ exciton energy (~ 1 mev for $p_{\tilde{y}}$ exciton) with the rotation angle. Interestingly, similar amplitude of the angular variation of the plasmon/exciton coupling has been found in the tunnelling electron-induced luminescence,[70] and in the theoretical study of the ZnPc molecule in plasmonic gap decorated with an atomic scale protrusions.[39]

Particularly well-resolved spatial information is revealed by the contour maps of the exciton energy differences shown in Fig. 7c). For large lateral separations the interaction with the nanoparticle and thus the exciton energy difference becomes small. Similarly, for a nanosphere located above the molecular center the exciton modes are degenerated with zero energy difference. When the nanoparticle is laterally displaced from the molecular center towards the carbon rings the degeneracy is lifted. The molecule/nanoparticle interaction leads to the up to 8 meV energy difference between the $p_{\tilde{x}}$ and $p_{\tilde{y}}$ eigenmodes, reflecting the orientation of the ZnPc end groups. Scans with gold nanospheres of both $D = 2$ nm and $D = 4$ nm diameter result in high contrasted images. Here, larger nanoparticle size leads to a zoom effect increasing the (x, y) extensions of molecular image, i.e. the range where the exciton/nanoparticle interaction is sensitive to the gross features of the spatial variation of the transition electron density.

We have also modelled the situation where the spherical metal nanoparticle scans the ZnPc molecule that is placed at the flat metal surface. This situation of the molecule in a plasmonic gap is typical for e.g. experimental setups where the dye molecule is deposited at a metal surface covered with an ionic crystal film and scanned by the tip of the scanning

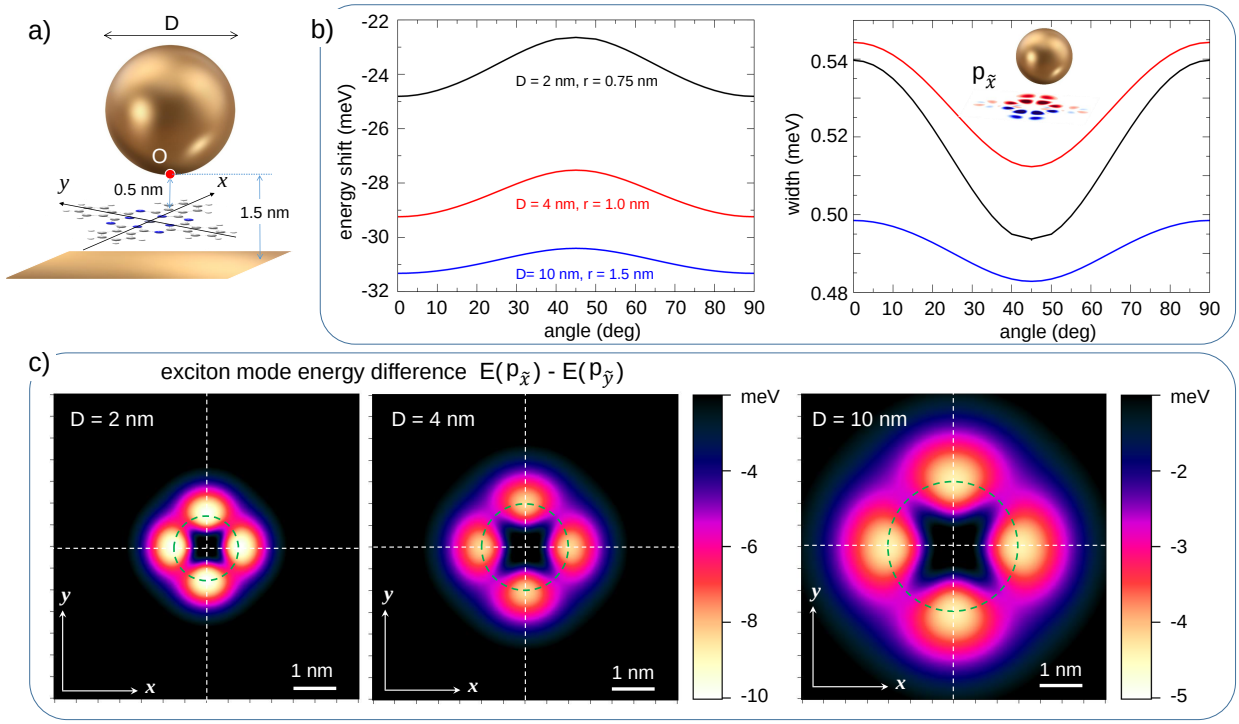

Figure 8: The plasmon gap geometry: ZnPc molecule is located in plasmon gap formed by the gold nanoparticle of diameter D and the gold surface. As sketched in panel a): The molecular plane is parallel to the surface and molecule/surface distane is 1 nm. The nanoparticle is moved in the plane parallel to the molecular plane. The separation between the molecular plane and the "analysis plane" is 0.5 nm. Panel b): The energy shift of the exciton with $p_{\tilde{x}}$ character from the transition in free-standing molecule (left), and the width of the $p_{\tilde{x}}$ exciton resonance owing to the non radiative decay rate because of the electron hole pair excitations in metal (right). Results obtained with different nanosphere diameter are shown as function of the rotation angle $\phi = \arctan(y/x)$ for the nanospere displaced along the circle of fixed radius $r = \sqrt{x^2 + y^2}$ as indicated with dashed green lines in panel c). The insert shows the transition charge density distribution of the $p_{\tilde{x}}$ exciton mode. Panel c): contour maps of the energy difference between the exciton modes with $p_{\tilde{x}}$ and $p_{\tilde{y}}$ character, $E_{p_{\tilde{x}}} - E_{p_{\tilde{y}}}$. Results are shown as function of the position of the $D = 2$ nm gold nanosphere (left image) and $D = 4$ nm gold nanosphere (middle image), and $D = 10$ nm gold nanosphere (right image). Green dashed circle indicates position of the gold nanosphere used for the plots in panel c).

tunneling microscope. The wide band gap ionic crystal film forms a spacer layer allowing to electronically decouple excited states of the molecule from the metal substrate. Thus, the spatial maps of the tunneling induced light emission from molecular excitons can be observed.[26,27,29–31,33,34,70–73] As shown in Fig. 8a, the ZnPc molecule is located in the plasmon gap formed by the gold nanoparticle of diameter D and the gold surface. The molecular plane

is parallel to the surface and the molecule/surface distane is 1 nm, mimicking the finite width of the spacer layer. The gold nanoparticle is moved in the plane separated by 0.5 nm from the molecular plane.

For the plasmon gap geometry we find very similar results to these reported in Fig. 7 for the molecule in vacuum scanned with a spherical metal nanoparticle. The in-plane extension of the molecular images is somewhat reduced, because the metal surface screens the potential owing to the excited electron density. As well, the presence of the metal surface leads to an additional energy shift and broadening of molecular excitons (see also Fig. 4). For the "probe" gold nanosphere following a circular trajectory of radius r around the center of the molecule, the exciton energies and widths display periodic variations with the rotation angle measured with respect to the molecular x- axis. For the $p_{\tilde{x}}$ exciton pointing towards the "probe" nanoparticle and primarily excited in experimental conditions because of the symmetry, we find that the exciton energy variation is of the order of $1-2$ meV. This value matches recent observations.[31,70] Good contrast in the contour maps showing the spatial profile of the exciton energy differences is obtained for the gold nanosphere as large as $D = 10$ nm in diameter, i.e. within the range of the sizes of the experimentally available "probes". This further illustrates the role of the self-interaction between the transition electron density associated with molecular excitations and the associated response potential of the nearby metallic nanoparticle. Information on the gross features of molecular structure can be gained without need of atomic size features at the metal surfaces across plasmonic gap.

We now discuss the possible effects regarding the atomic structure of the metal surface and/or metal nanoparticle. As pointed out in the introduction, the recent interest to the properties of molecular excitons in narrow plasmonic gaps and/or close to the metal surface is triggered by experimental studies with atomic size resolution reached by using scanning AFM and STM techniques.[26,27,29–33,70,72,73] In these devices, the molecule is physisorbed at a buffer oxide or ionic crystal layer. The buffer layer decouples the electronic states of the molecular

emitter from those of the metal substrate, and allows to avoid loss of the excited electron into the metal. In the physisorption conditions, the perturbation of the molecular structure by the interaction with surface atoms is small.[74] This explains the success in the interpretation of the above experimental data using gas-phase electronic and vibronic structure of the molecule, as well as this supports the present approach. Obviously, the presence of surface adatoms or steps might lead to a hybridization of the excited states comparable to the effect of the induced potentials discussed in this paper. In this respect it might be very interesting to conduct experiments on light emission from molecular excitons purposely placing the molecule close to the surface imperfections. At the same time, using scanning AFM and STM techniques the experiments can be controllably performed on perfect surface terraces as considered here.

It is also worth to stress that high spatial resolution is achieved in the present work partly thanks to the relatively large size of the ZhPc dye molecule. Depending on the molecular size, the effect would vary quantitatively. However, qualitatively it will persist since it is based on the robust consequences of molecular electronic structure.

Conclusions and outlook

In conclusion, we have shown that, for quantum emitters interacting with plasmonic systems, the molecular scale sensitivity of the exciton coupling with metal nanoparticles could be observed without tight spatial localization of the plasmon fields by e.g. atomic scale protrutions. The effect is present when the distance between the molecular quantum emitter and metal surface becomes comparable to molecular dimensions, and it is operative even for flat metal surfaces. It follows from our results that the quantum emitter plays simultaneously the role of source and probe of the localized fields created by the system in response to its own presence.

Molecular scale resolution stems from the finite spatial extension of the excited charge

density associated with molecular excitons, and from the corresponding non dipolar terms in the near field. It is not captured by the standard point dipole approximation for the QE interacting with plasmonic nanoparticles. To account for the finite spatial extension of the excited charge density requires a quantum description as employed here.

We have shown that mapping of molecular excitons with a plasmonic nanoparticle of several nm size reveals the gross features of the atomic arrangement in the molecule. In the D_{4h} symmetry case of the planar ZnPc molecule interacting with plasmonic nanoparticle, the calculated variation of the exciton energies with in-plane orientation of the molecular axis is consistent with recent experimental observations.[70] We have also demonstrated the possibility of polarization conversion at exciton resonances owing to the near field effects.

Our findings are of fundamental importance for e.g. interpretation of atomically resolved molecular luminescence triggered by electron tunneling in STM device. As well, the possibility the atomic scale control of molecular excitons in a plasmonic environment have implications for practical issues such as design of single photon sources, molecular detection and spectroscopy, nonlinear applications and photochemistry.

Acknowledgement

We acknowledge the generous allocation of computer time at the Centro de Computación Científica at the Universidad Autonóma de Madrid (CCC-UAM). This work was partially supported by the project CTQ2016-76061-P of the Spanish Ministerio de Economía y Competitividad (MINECO). F.A.G. acknowledges the FPI grant associated with the project CTQ2013-43698-P (MINECO). Financial support from the MINECO through the "María de Maeztu" Program for Units of Excellence in R&D (MDM-2014-0377) is also acknowledged.

Supporting Information Available

The following files are available free of charge.

Supporting information providing details on the

- Point dipole approximation,
- Role of the plasmon modes,
- Quantum approach proposed for molecular excitons,
- *Ab initio* quantum chemistry methods used for the ground state and excited state of the free-standing ZhPc molecule,
- Polarization conversion in the system.

References

(1) Carminati, R.; Greffet, J.-J.; Henkel, C.; J.M.Vigoureux, Radiative and non-radiative decay of a single molecule close to a metallic nanoparticle. *Optics Communications* **2006**, *261*, 368–375.

(2) Delga, A.; Feist, J.; Bravo-Abad, J.; Garcia-Vidal, F. J. Quantum emitters near a metal nanoparticle: strong coupling and quenching. *Phys. Rev. Lett.* **2014**, *112*, 253601.

(3) Carminati, R.; Cazé, A.; Cao, D.; Peragut, F.; Krachmalnicoff, V.; Pierrat, R.; Wilde, Y. D. Electromagnetic density of states in complex plasmonic systems. *Surface Science Reports* **2015**, *70*, 1–41.

(4) Ayala-Orozco, C.; Liu, J. G.; Knight, M. W.; Wang, Y.; Day, J. K.; Nordlander, P.; Halas, N. J. Fluorescence enhancement of molecules inside a gold nanomatryoshka. *Nano Letters* **2014**, *14*, 2926–2933.

(5) Cacciola, A.; Di Stefano, O.; Stassi, R.; Saija, R.; Savasta, S. Ultrastrong coupling of plasmons and excitons in a nanoshell. *ACS Nano* **2014**, *8*, 11483–11492.

(6) Muljarov, E. A.; Langbein, W. Exact mode volume and Purcell factor of open optical systems. *Phys. Rev. B* **2016**, *94*, 235438.

(7) Haran, G.; Chuntonov, L. Artificial plasmonic molecules and their interaction with real molecules. *Chemical Reviews* **2018**, *118*, 5539–5580.

(8) Vasa, P.; Lienau, C. Strong light - matter interaction in quantum emitter/metal hybrid nanostructures. *ACS Photonics* **2018**, *5*, 2–23.

(9) Manjavacas, A.; García de Abajo, F. J.; Nordlander, P. Quantum plexcitonics: strongly interacting plasmons and excitons. *Nano Letters* **2011**, *11*, 2318–2323.

(10) Belacel, C.; Habert, B.; Bigourdan, F.; Marquier, F.; Hugonin, J.-P.; Michaelis de Vasconcellos, S.; Lafosse, X.; Coolen, L.; Schwob, C.; Javaux, C.; Dubertret, B.; Greffet, J.-J.; Senellart, P.; Maitre, A. Controlling spontaneous emission with plasmonic optical patch antennas. *Nano Letters* **2013**, *13*, 1516–1521.

(11) Schlather, A. E.; Large, N.; Urban, A. S.; Nordlander, P.; Halas, N. J. Near - field mediated plexcitonic coupling and giant rabi splitting in individual metallic dimers. *Nano Letters* **2013**, *13*, 3281–3286.

(12) Chikkaraddy, R.; de Nijs, B.; Benz, F.; Barrow, S. J.; Scherman, O. A.; Rosta, E.; Demetriadou, A.; Fox, P.; Baumberg, J. J. Single-molecule strong coupling at room temperature in plasmonic nanocavities. *Nature* **2016**, *535*, 127.

(13) Benz, F.; Schmidt, M. K.; Dreismann, A.; Chikkaraddy, R.; Zhang, Y.; Demetriadou, A.; Carnegie, C.; Ohadi, H.; de Nijs, B.; Esteban, R.; Aizpurua, J.; Baumberg, J. J. Single-molecule optomechanics in picocavities. *Science* **2016**, *354*, 726–729.

(14) Chen, X.; Chen, Y.-H.; Qin, J.; Zhao, D.; Ding, B.; Blaikie, R. J.; Qiu, M. Mode modification of plasmonic gap resonances induced by strong coupling with molecular excitons. *Nano Letters* **2017**, *17*, 3246–3251.

(15) Sun, J.; Hu, H.; Zheng, D.; Zhang, D.; Deng, Q.; Zhang, S.; Xu, H. Light - emitting plexciton: exploiting plasmon - exciton interaction in the intermediate coupling regime. *ACS Nano* **2018**, *12*, 10393–10402.

(16) Cuadra, J.; Baranov, D. G.; Wersäll, M.; Verre, R.; Antosiewicz, T. J.; Shegai, T. Observation of tunable charged excito polaritons in hybrid monolayer WS2 - plasmonic nanoantenna system. *Nano Letters* **2018**, *18*, 1777–1785.

(17) Santhosh, K.; Bitton, O.; Chuntonov, L.; Haran, G. Vacuum Rabi splitting in a plasmonic cavity at the single quantum emitter limit. *Nature Communications* **2016**, *7*, 11823.

(18) Groß, H.; Hamm, J. M.; Tufarelli, T.; Hess, O.; Hecht, B. Near-field strong coupling of single quantum dots. *Science Advances* **2018**, *4*.

(19) Leng, H.; Szychowski, B.; Daniel, M.-C.; Pelton, M. Strong coupling and induced transparency at room temperature with single quantum dots and gap plasmons. *Nature Communications* **2018**, *9*, 4012.

(20) Feist, J.; Galego, J.; Garcia-Vidal, F. J. Polaritonic chemistry with organic molecules. *ACS Photonics* **2018**, *5*, 205–216.

(21) Zhang, W.; Cui,; Yeo, B.-S.; Schmid, T.; Hafner, C.; Zenobi, R. Nanoscale roughness on metal surfaces can increase tip-enhanced Raman scattering by an order of magnitude. *Nano Letters* **2007**, *7*, 1401–1405.

(22) Zhang, R.; Zhang, Y.; Dong, Z. C.; Jiang, S.; Zhang, C.; Chen, L. G.; Zhang, L.; Liao, Y.; Aizpurua, J.; Luo, Y.; Yang, J. L.; Hou, J. G. Chemical mapping of a single molecule by plasmon-enhanced Raman scattering. *Nature* **2013**, *498*, 82.

(23) Jiang, S.; Zhang, Y.; Zhang, R.; Hu, C.; Liao, M.; Luo, Y.; Yang, J.; Dong, Z.; Hou, J. G.

Distinguishing adjacent molecules on a surface using plasmon-enhanced Raman scattering. *Nature Nanotechnology* **2015**, *10*, 865.

(24) Chiang, N.; Chen, X.; Goubert, G.; Chulhai, D. V.; Chen, X.; Pozzi, E. A.; Jiang, N.; Hersam, M. C.; Seideman, T.; Jensen, L.; Van Duyne, R. P. Conformational contrast of surface - mediated molecular switches yields angstrom-scale spatial resolution in ultrahigh vacuum tip-enhanced Raman spectroscopy. *Nano Letters* **2016**, *16*, 7774–7778.

(25) Tallarida, N.; Lee, J.; Apkarian, V. A. Tip-enhanced raman Spectromicroscopy on the angstrom scale: bare and CO-terminated Ag tips. *ACS Nano* **2017**, *11*, 11393–11401.

(26) Wu, S. W.; Nazin, G. V.; Ho, W. Intramolecular photon emission from a single molecule in a scanning tunneling microscope. *Phys. Rev. B* **2008**, *77*, 205430.

(27) Chen, C.; Chu, P.; Bobisch, C. A.; Mills, D. L.; Ho, W. Viewing the interior of a single molecule: vibronically resolved photon imaging at submolecular resolution. *Phys. Rev. Lett.* **2010**, *105*, 217402.

(28) Große, C.; Kabakchiev, A.; Lutz, T.; Froidevaux, R.; Schramm, F.; Ruben, M.; Etzkorn, M.; Schlickum, U.; Kuhnke, K.; Kern, K. Dynamic control of plasmon generation by an individual quantum system. *Nano Letters* **2014**, *14*, 5693–5697.

(29) Doppagne, B.; Chong, M. C.; Bulou, H.; Boeglin, A.; Scheurer, F.; Schull, G. Electrofluorochromism at the single-molecule level. *Science* **2018**, *361*, 251–255.

(30) Doppagne, B.; Chong, M. C.; Lorchat, E.; Berciaud, S.; Romeo, M.; Bulou, H.; Boeglin, A.; Scheurer, F.; Schull, G. Vibronic spectroscopy with submolecular resolution from STM-induced electroluminescence. *Phys. Rev. Lett.* **2017**, *118*, 127401.

(31) Imada, H.; Miwa, K.; Imai-Imada, M.; Kawahara, S.; Kimura, K.; Kim, Y. Single-

molecule investigation of energy dynamics in a coupled plasmon-exciton system. *Phys. Rev. Lett.* **2017**, *119*, 013901.

(32) Zhang, L.; Yu, Y.-J.; Chen, L.-G.; Luo, Y.; Yang, B.; Kong, F.-F.; Chen, G.; Zhang, Y.; Zhang, Q.; Luo, Y.; Yang, J.-L.; Dong, Z.-C.; Hou, J. G. Electrically driven single-photon emission from an isolated single molecule. *Nature Communications* **2017**, *8*, 580.

(33) Rossel, F.; Pivetta, M.; Schneider, W.-D. Luminescence experiments on supported molecules with the scanning tunneling microscope. *Surface Science Reports* **2010**, *65*, 129–144.

(34) Kuhnke, K.; Große, C.; Merino, P.; Kern, K. Atomic-scale imaging and spectroscopy of electroluminescence at molecular interfaces. *Chemical Reviews* **2017**, *117*, 5174–5222.

(35) Tersoff, J.; Hamann, D. R. Theory of the scanning tunneling microscope. *Phys. Rev. B* **1985**, *31*, 805–813.

(36) Hofer, W. A.; Foster, A. S.; Shluger, A. L. Theories of scanning probe microscopes at the atomic scale. *Rev. Mod. Phys.* **2003**, *75*, 1287–1331.

(37) Trautmann, S.; Aizpurua, J.; Götz, I.; Undisz, A.; Dellith, J.; Schneidewind, H.; Rettenmayr, M.; Deckert, V. A classical description of subnanometer resolution by atomic features in metallic structures. *Nanoscale* **2017**, *9*, 391–401.

(38) Liu, P.; Chulhai, D. V.; Jensen, L. Single - molecule imaging using atomistic near-field tip-enhanced Raman spectroscopy. *ACS Nano* **2017**, *11*, 5094–5102.

(39) Neuman, T.; Esteban, R.; Casanova, D.; García-Vidal, F. J.; Aizpurua, J. Coupling of molecular emitters and plasmonic cavities beyond the point-dipole approximation. *Nano Letters* **2018**, *18*, 2358–2364.

(40) Romero, I.; Aizpurua, J.; Bryant, G. W.; de Abajo, F. J. G. Plasmons in nearly touchingmetallic nanoparticles: singular response in the limit of touching dimers. *Opt. Express* **2006**, *14*, 9988–9999.

(41) Barbry, M.; Koval, P.; Marchesin, F.; Esteban, R.; Borisov, A. G.; Aizpurua, J.; Sánchez-Portal, D. Atomistic near-field nanoplasmonics: reaching atomic-scale resolution in nanooptics. *Nano Letters* **2015**, *15*, 3410–3419.

(42) Ren, X.; Rinke, P.; Joas, C.; Scheffler, M. Random-phase approximation and its applications in computational chemistry and materials science. *Journal of Materials Science* **2012**, *47*, 7447–7471.

(43) Marques, M. A. L.; Gross, E. K. U. Time-dependent density functional theory. *Annu. Rev. Phys. Chem.* **2004**, *55*, 427–455.

(44) Burke, K.; Werschnik, J.; Gross, E. K. U. Time-dependent density functional theory: Past, present, and future. *The Journal of Chemical Physics* **2005**, *123*, 062206.

(45) Morawitz, H. Self-coupling of a two-level system by a mirror. *Phys. Rev.* **1969**, *187*, 1792–1796.

(46) Chance, R. R.; Prock, A.; Silbey, R. Lifetime of an excited molecule near a metal mirror: Energy transfer in the Eu3+/silver system. *The Journal of Chemical Physics* **1974**, *60*, 2184–2185.

(47) Ford, G.; Weber, W. Electromagnetic interactions of molecules with metal surfaces. *Physics Reports* **1984**, *113*, 195–287.

(48) Lopata, K.; Neuhauser, D. Nonlinear nanopolaritonics: Finite-difference time-domain Maxwell - Schrödinger simulation of molecule-assisted plasmon transfer. *The Journal of Chemical Physics* **2009**, *131*, 014701.

(49) Salomon, A.; Gordon, R. J.; Prior, Y.; Seideman, T.; Sukharev, M. Strong coupling between molecular excited states and surface plasmon modes of a slit array in a thin metal film. *Phys. Rev. Lett.* **2012**, *109*, 073002.

(50) Sukharev, M.; Nitzan, A. Optics of exciton-plasmon nanomaterials. *Journal of Physics: Condensed Matter* **2017**, *29*, 443003.

(51) Corni, S.; Tomasi, J. Excitation energies of a molecule close to a metal surface. *The Journal of Chemical Physics* **2002**, *117*, 7266–7278.

(52) Corni, S.; Tomasi, J. Lifetimes of electronic excited states of a molecule close to a metal surface. *The Journal of Chemical Physics* **2003**, *118*, 6481–6494.

(53) Andreussi, O.; Corni, S.; Mennucci, B.; Tomasi, J. Radiative and nonradiative decay rates of a molecule close to a metal particle of complex shape. *The Journal of Chemical Physics* **2004**, *121*, 10190–10202.

(54) Morton, S. M.; Silverstein, D. W.; Jensen, L. Theoretical studies of plasmonics using electronic structure methods. *Chemical Reviews* **2011**, *111*, 3962–3994.

(55) Payton, J. L.; Morton, S. M.; Moore, J. E.; Jensen, L. A hybrid atomistic electrodynamics-quantum mechanical approach for simulating surface-enhanced Raman scattering. *Accounts of Chemical Research* **2014**, *47*, 88–99.

(56) Nascimento, D. R.; DePrince, A. E. Modeling molecule-plasmon interactions using quantized radiation fields within time-dependent electronic structure theory. *The Journal of Chemical Physics* **2015**, *143*, 214104.

(57) Fihey, A.; Maurel, F.; Perrier, A. Plasmon-excitation coupling for Dithienylethene/Gold nanoparticle hybrid systems: a theoretical study. *The Journal of Physical Chemistry C* **2015**, *119*, 9995–10006.

(58) Pipolo, S.; Corni, S. Real-time description of the electronic dynamics for a molecule close to a plasmonic nanoparticle. *The Journal of Physical Chemistry C* **2016**, *120*, 28774–28781.

(59) Frisch, M. J. et al. Gaussian 09 Revision E.01. 2013; Gaussian Inc. Wallingford CT 2013.

(60) Heyd, J.; Scuseria, G. E. Efficient hybrid density functional calculations in solids: assessment of the Heyd-Scuseria-Ernzerhof screened Coulomb hybrid functional. *The Journal of Chemical Physics* **2004**, *121*, 1187–1192.

(61) Heyd, J.; Peralta, J. E.; Scuseria, G. E.; Martin, R. L. Energy band gaps and lattice parameters evaluated with the Heyd-Scuseria-Ernzerhof screened hybrid functional. *The Journal of Chemical Physics* **2005**, *123*, 174101.

(62) Heyd, J.; Scuseria, G. E.; Ernzerhof, M. Erratum: "Hybrid functionals based on a screened Coulomb potential" [J. Chem. Phys. 118, 8207 (2003)]. *The Journal of Chemical Physics* **2006**, *124*, 219906.

(63) Ordal, M. A.; Long, L. L.; Bell, R. J.; Bell, S. E.; Bell, R. R.; Alexander, R. W.; Ward, C. A. Optical properties of the metals Al, Co, Cu, Au, Fe, Pb, Ni, Pd, Pt, Ag, Ti, and W in the infrared and far infrared. *Appl. Opt.* **1983**, *22*, 1099–1119.

(64) Johnson, P. B.; Christy, R. W. Optical constants of the noble metals. *Phys. Rev. B* **1972**, *6*, 4370–4379.

(65) Marinica, D. C.; Lourenço-Martins, H.; Aizpurua, J.; G., B. A. Plexciton quenching by resonant electron transfer from quantum emitter to metallic nanoantenna. *Nano Letters* **2013**, *13*, 5972–5978.

(66) Los, J.; Geerlings, J. Charge exchange in atom-surface collisions. *Physics Reports* **1990**, *190*, 133–190.

(67) Luk'yanchuk, B.; Zheludev, N. I.; Maier, S. A.; Halas, N. J.; Nordlander, P.; Giessen, H.; Chong, C. T. The Fano resonance in plasmonic nanostructures and metamaterials. *Nature Materials* **2010**, *9*, 707.

(68) Hao, F.; Sonnefraud, Y.; Dorpe, P. V.; Maier, S. A.; Halas, N. J.; Nordlander, P. Symmetry breaking in plasmonic nanocavities: subradiant LSPR sensing and a tunable fano resonance. *Nano Letters* **2008**, *8*, 3983–3988.

(69) Zhang, C.; Chen, B.-Q.; Li, Z.-Y. Optical origin of subnanometer resolution in tip-enhanced raman mapping. *The Journal of Physical Chemistry C* **2015**, *119*, 11858–11871.

(70) Zhang, Y.; Meng, Q.-S.; Zhang, L.; Luo, Y.; Yu, Y.-J.; Yang, B.; Zhang, Y.; Esteban, R.; Aizpurua, J.; Luo, Y.; Yang, J.-L.; Dong, Z.-C.; Hou, J. G. Sub-nanometre control of the coherent interaction between a single molecule and a plasmonic nanocavity. *Nature Communications* **2017**, *8*, 15225.

(71) Lee, J.; Perdue, S. M.; Rodriguez Perez, A.; Apkarian, V. A. Vibronic motion with joint angstromâĂŞfemtosecond resolution observed through Fano progressions recorded within one molecule. *ACS Nano* **2014**, *8*, 54–63.

(72) Zhang, Y.; Luo, Y.; Zhang, Y.; Yu, Y.-J.; Kuang, Y.-M.; Zhang, L.; Meng, Q.-S.; Luo, Y.; Yang, J.-L.; Dong, Z.-C.; Hou, J. G. Visualizing coherent intermolecular dipoleâĂŞdipole coupling in real space. *Nature* **2016**, *531*, 623.

(73) Imada, H.; Miwa, K.; Imai-Imada, M.; Kawahara, S.; Kimura, K.; Kim, Y. Real-space investigation of energy transfer in heterogeneous molecular dimers. *Nature* **2016**, *538*, 364.

(74) Robledo, M.; Pacchioni, G.; Martín, F.; Alcamí, M.; Díaz-Tendero, S. Adsorption of Benzene on Cu(100) and on Cu(100) covered with an ultrathin NaCl film: molecule-

substrate interaction and decoupling. *The Journal of Physical Chemistry C* **2015**, *119*, 4062–4071.

Graphical TOC Entry